Design and Prototyping of a Cable-Driven Parallel Robot with a Reconfigurable Moving-Platform for Pick-and-Place Operations

Camillo Murgia, Philip Long, Stéphane Caro

Design and Prototyping of a Cable-Driven Parallel Robot with a Reconfigurable Moving-Platform for Pick-and-Place Operations

Camillo Murgia[1,2], Philip Long[2], Stéphane Caro[1]

***Abstract*— Operating traditional serial robots in large environments are challenging due to the difficulty and exponential cost of scaling the system's workspace. Cable-Driven Parallel Robots (CDPRs), thanks to the low cost of cables in comparison to more sophisticated mechanisms, have the possibility to operate across large workspaces with limited cost. However, one issue for CDPR remains the more complex handling of cable collisions with the environment, in particular when operating in cluttered environments that are typical in large warehouses. The following work presents a solution to this problem through the use of a reconfigurable Mobile Platform. The mechanical design and control strategy are proposed and discussed. A reconfigurable dual-platform design and unique cable routing inside the CDPR's mobile platform make it possible to increase the robot reachability. Using only the main robot motors and a docking system between the mobile platform and the work-cell ceiling, the system can dock throughout the entire workspace and deploy a sub-robot capable of operating between obstacles increasing the reachability of the robot. Two different docking system design are tested using dedicated control strategy and compared. The prototypes are experimentally validated and compared using a large scale eight cables CDPR.**

I. INTRODUCTION

The use of cables to provide the actuation of robots is an attractive prospect due to the advantages of lightweight structure and low energy consumption across large space. This work focuses on a particular class of cable robot, known as Cable-Driven Parallel Robot (CDPR). The general structure of a CDPR, presented in [1], is similar to a steward platform [2], where the links are in this case cables. A fixed structure act as the supports for the cables and the actuators of the robot, while a mobile platform ($\mathcal{MP}$) connected to the cables can move as a function of the length of the cables. The cable length vector describes the state of the robot. Each cable acts as a limb of the robot. The number of the cables define the controllable DOFs of the $\mathcal{MP}$ and due to the nature of cables i.e. they cannot push, a redundant number of cables is necessary in order to achieve 6 DOF, in particular eight cables are used. CDPRs thanks to the light structure provided by the cables can guarantee a large workspace.

We focus on suspended CDPRs where the $\mathcal{MP}$ is suspended from the top structure via attachment points, thus reducing potential collisions in the environment. In the field of CDPRs, particularly suspended CDPRs, the ability to span a large workspace both horizontally and vertically makes them suitable for a wide range of pick and place (P&P) tasks. The use of cables in the robot's actuation allows for a relatively lightweight $\mathcal{MP}$, with the weight of the motors placed on the robot's external frame, significantly reducing the $\mathcal{MP}$'s inertia.

However, cable collisions still present a major challenge when operating in a cluttered environment. In a P&P scenario within a large warehouse with tall shelves or piles of boxes, the workspace of a traditional suspended CDPR is often limited due to possible collisions with tall obstacles while the $\mathcal{MP}$ is attempting to reach a position at the bottom of the workspace. This limitation can significantly compromise the applicability of this type of robot in cluttered environments. A solution that utilizes a reconfigurable $\mathcal{MP}$, consisting of a main and a secondary platform that can be deployed by the main one, is presented in Skopin *et al.* work [3].

In this work, key features focusing on the interface between the main and the secondary platforms, and the docking system functionalities are re-designed and a tension distribution switching controller implemented. The approach is validated using the CRAFT robot, an eight cable suspended-CDPR. The paper is organized as follows: Section II presents related works on CDPR, Section III presents the mechanical structure of the $\mathcal{MP}$ and its modelling, focusing on cables routing, the interface between the main and secondary platforms, and the docking system. Section IV describes the control strategy used to operate the CDPR. Section V presents the experimental results conducted with the new design. Section VI draws conclusions and outlines future work.

II. RELATED WORK

CDPRs have been used in several different applications, both outdoor and indoor, notably, Skycam [4], where a four-cable CDPR is used to move a camera inside a stadium for aerial videos of sports matches or events. Other outdoor applications are related to the assembly of large solar panels [5] or the actuation of large radio telescopes such as the FAST [6], or in a vertical planar configuration to automate the cleaning of large glass walls [7]. In indoor applications, CDPRs have been used in various configurations for visual inspection [8] or object handling. P&P of heavy metal part is performed in [9] using a reconfigurable CDPR in which the position of the pulleys can be modified in a discrete manner on its frame. CDPR is used in [10] to test cables that can detect collisions with humans, in order to create a safe environment for human-robot collaboration. In

This work is supported by ANR CRAFT project, France, grant ANR-18-CE10-0004, https://anr.fr/Project-ANR-18-CE10-0004 and ROBOTEX 2.0 (ROBOTEX ANR-10-EQPX-44-01 and TIRREX ANR-21-ESRE-0015).

[1] Nantes Université - Ecole Centrale de Nantes, CNRS, LS2N, UMR 6004, F-4400 Nantes, France stephane.caro@ls2n.fr

[2] ATU Galway City, Ireland camillo.murgia@atu.ie, philip.long@atu.ie

[11], a CDPR is used in additive manufacturing to have a lightweight $\mathcal{MP}$ capable of moving the material extruder for 3D printing. Various solutions have been proposed for interacting with objects on large shelves in warehouses, a planar robot capable of operating on the side of a shelf is presented in [12]. In [13] a more versatile mobile CDPR is presented, capable of moving inside a warehouse as a mobile robot, and then, thanks to two mobile units where the cables are attached, it can deploy an $\mathcal{MP}$ that can operate in a planar workspace next to a shelf.

CDPR design places significant importance on its workspace. In [14], the workspace is considered the robot's primary design parameter. A detailed explanation of the workspace of a CDPR is presented in [15]. The article discusses the importance and computation of the Wrench Feasible Workspace (WFW). Several studies have addressed the computation of the WFW for traditional CDPR [16], as well as for reconfigurable CDPRs, such as mobile-CDPRs [17] or planar reconfigurable CDPRs with a parent and a child $\mathcal{MP}$ [18].

The design presented in this work, thanks to its novel reconfigurable platform, is intended to increase its effectiveness within a logistics warehouse or distribution center. In particular, where a different CDPR configuration would not be able to operate due to the cluttered environment and other solutions such as more conventional mobile robots would not be suitable.

III. RECONFIGURABLE DESIGN

A. Mechanical Design of the $\mathcal{MP}$

The proposed $\mathcal{MP}$ is used on the CRAFT robot which has an external structure measuring $3.75 \times 4.35 \times 2.75$ meter and supports all motors, winches, and pulleys. In this work, all 8 pulleys that provide the fixed exit points for the cables, are placed near the ceiling, with two pulleys at each corner. Table I provides details on the exact exit points.

The $\mathcal{MP}$ consists of a main platform $\mathcal{P}_1$ and a secondary platform $\mathcal{P}_2$ see Fig. 1. Both platforms are made using 20×20 millimeter aluminum profiles. $\mathcal{P}_1$ is composed by an external frame $50 \times 50 \times 30$ centimeter made of aluminum, on the lower side a 3D printed plastic piece act as interface with the $\mathcal{P}_2$. On the platform's upper side, two aluminum bars are used to mount on the docking system. $\mathcal{P}_2$ is made up of a 15×15 centimeter square aluminum structure with four 3D

TABLE I: Anchor points of the cables between the CRAFT frame and the main $\mathcal{MP}$. On the left, the pulley exit points of the cables in the fixed robot frame. On the right the anchor points of the main platform $\mathcal{P}_1$ in its own frame. index i represent the cables number. All the values are in meter.

i	${}^{\mathcal{F}}\mathbf{a}_i$			${}^{\mathcal{P}_1}\mathbf{b}_i$		
	x	y	z	x	y	z
1	0.379	0.008	2.780	0.240	-0.251	0.294
2	0.059	0.314	2.778	-0.259	0.238	0.010
3	0.054	3.934	2.778	-0.251	-0.240	0.294
4	0.366	4.249	2.785	0.238	0.259	0.010
5	3.378	4.254	2.787	-0.240	0.251	0.294
6	3.690	3.951	2.788	0.259	-0.238	0.010
7	3.695	0.317	2.788	0.251	0.240	0.294
8	3.386	0.009	2.783	-0.238	-0.259	0.010

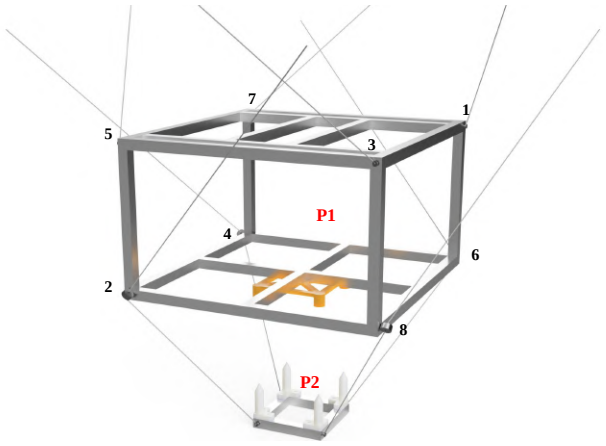

(a) Render of both the moving platforms. The two $\mathcal{MP}s$ are not in contact in this case. It is possible to see the cables anchor points and the eyelets that route the cables to the $\mathcal{P}_2$. Each anchor points is numbered with respect to the cables enumeration convention used in this CDPR.

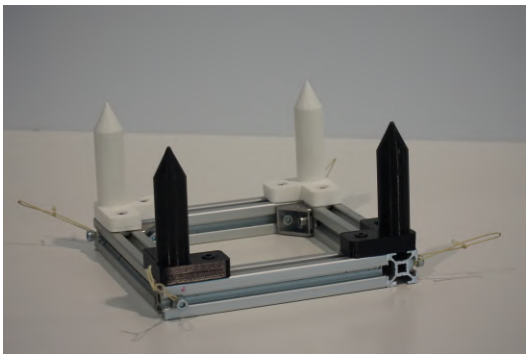

(b) $\mathcal{P}_2$ the four big pins are part of the interface with the $\mathcal{P}_1$.

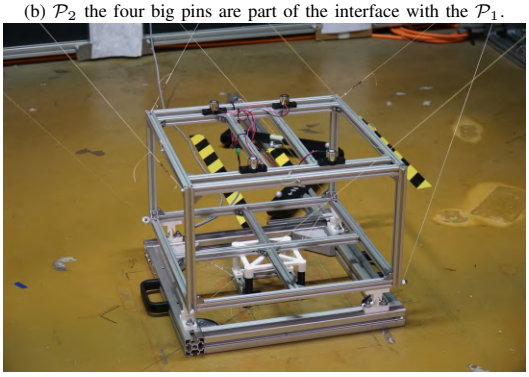

(c) Photo of both $\mathcal{P}_1$ and $\mathcal{P}_2$ with the two platform in contact.

Fig. 1: Design of the Dual-Platform prototype presented in this work.

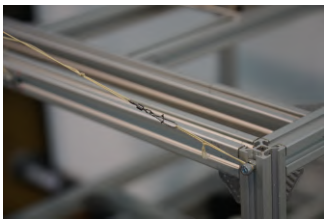

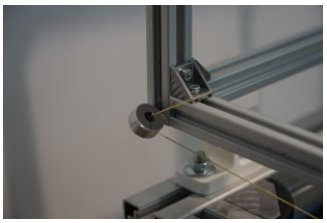

Fig. 2: Close up of the fixed anchor points and the eyelets mounted on $\mathcal{P}_1$.

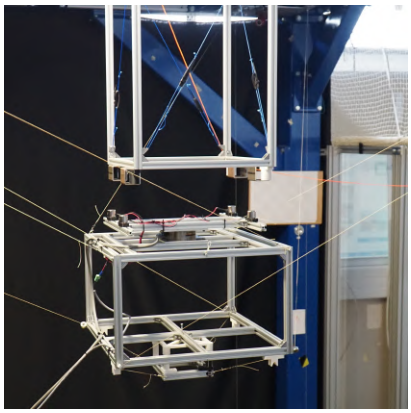

(a) Operational mode 1, the $\mathcal{MP}$ ($\mathcal{P}_1 \cup \mathcal{P}_2$) is free to move within the workspace.

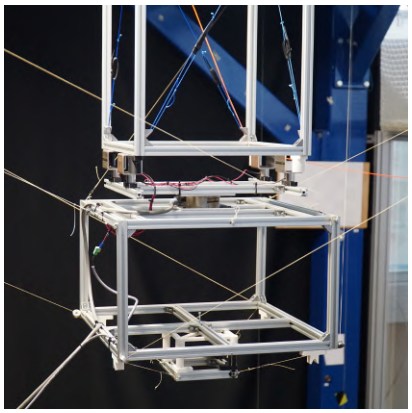

(b) Operational mode 2, $\mathcal{P}_1$ is attached to the ceiling thanks to the docking system, $\mathcal{P}_2$ is still in contact to $\mathcal{P}_1$.

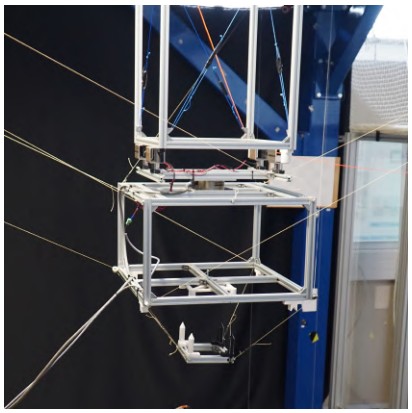

(c) Operational mode 3, $\mathcal{P}_1$ is docked, $\mathcal{P}_2$ is free to move in its sub-workspace.

Fig. 3: Different operational modes of the robot.

(a) Top view of the $\mathcal{MP}$ with the four pins installed.

(b) Render of the two components of the pin/socket system.

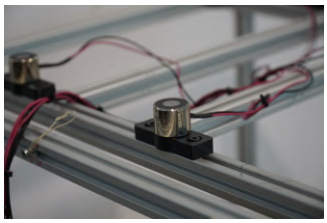

(c) Close up of a single electromagnet. Each electromagnet is held in position by a small 3D printed support (in black).

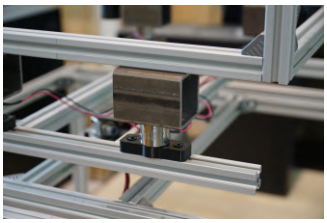

(d) Close up of the interface between the electromagnet and the metallic fixed docking part.

Fig. 4: Details of the two presented docking system.

printed pins pointing upward that act as contact points with $\mathcal{P}_1$. The eight cables used to operate the $\mathcal{MP}$ are anchored according to this scheme:

- cables 1, 3, 5, and 7 are fixed to the four upper corners of $\mathcal{P}_1$
- cables 2, 4, 6, and 8 are free to pass through loops fixed to the four lower corners of $\mathcal{P}_1$ and then fixed to the four corners of $\mathcal{P}_2$

The position of $\mathcal{P}_1$'s connection points are given in Table I. The fixed cable connection to the $\mathcal{MP}$ consists of a small cable loop fixed on the $\mathcal{MP}$, and a hook attached to the end of each cable. The four eyelets on the $\mathcal{P}_1$ are made of a simple cylindrical piece of machined aluminum with a hole in the center through which the cable can pass freely Fig. 2.

B. Kinetostatic model of CDPR

To simplify the robot description, a model based on the static equilibrium of the $\mathcal{MP}$ is introduced. A frame $\mathscr{F}$ is attached to the system's fixed structure, and a frame $\mathscr{P}$ to the $\mathcal{MP}$ with respective origins O and P. The pose of $\mathcal{MP}$ is defined in the frame $\mathscr{F}$ as a vector $\mathbf{p}$ and a rotation matrix $\mathbf{Q}$, illustrated in Fig. 5. Each cable is modeled as a straight line with negligible mass and inelastic properties. It is identified by a vector $\mathbf{c}_i$ and its norm is c_i. The anchor points of the cables are denoted as A_i and vector $\mathbf{a}_i$ w.r.t. frame $\mathscr{F}$ and B_i and vector $\mathbf{r}_i$ w.r.t. frame $\mathscr{P}$. An external wrench applied to the $\mathcal{MP}$ is defined as $\mathbf{w}_e$, and the tension in each i-th cables is defined as the vector $\mathbf{t}$. The static equilibrium of the $\mathcal{MP}$ can be described by the equation:

$$\mathbf{W}\mathbf{t} + \mathbf{w}_e = \mathbf{0}_6 \tag{1}$$

Where the matrix $\mathbf{W}$ is the wrench matrix defined as:

$$\mathbf{W} = \begin{bmatrix} \mathbf{c}_1/c_1 & \cdots & \mathbf{c}_m/c_m \\ (\mathbf{Q}\mathbf{r}_1) \times \mathbf{c}_1/(rc_1) & \cdots & (\mathbf{Q}\mathbf{r}_m) \times \mathbf{c}_m/(rc_m) \end{bmatrix} \tag{2}$$

Using the matrix $\mathbf{W}$ it is possible to derive both the geometric and kinematic model of the CDPR. The robot's state variables are defined as the vector $\mathbf{q}$ describing the joint position, and $\mathbf{x}$ describing the Cartesian pose of the $\mathcal{MP}$. The twist (pose time derivative) of the $\mathcal{MP}$ is defined as $\dot{\mathbf{x}}$.

C. $\mathcal{MP}$ Operational Modes

It is possible to identify three different configurations of the overall reconfigurable $\mathcal{MP}$ during its operation, following the definition presented in [18]

- **Operational Mode 1** ($\mathcal{OM}_1$) the two $\mathcal{MP}s$ $\mathcal{P}_1$ and $\mathcal{P}_2$ are stuck together (due to the higher mass of $\mathcal{P}_1$ that exerts a force against $\mathcal{P}_2$, and the interface between $\mathcal{P}_1$ and $\mathcal{P}_2$ that prevents from xy plane translation and xyz rotation). The whole platform behaves as a single platform with eight cables in COGIRO like configuration [19]. The $\mathcal{MP}$ can move freely within the workspace, and is defined as $\mathcal{MP} = \mathcal{P}_1 \cup \mathcal{P}_2$. The twist of the two platform is the same: $\dot{\mathbf{x}}_1 = \dot{\mathbf{x}}_2 = \dot{\mathbf{x}}$,

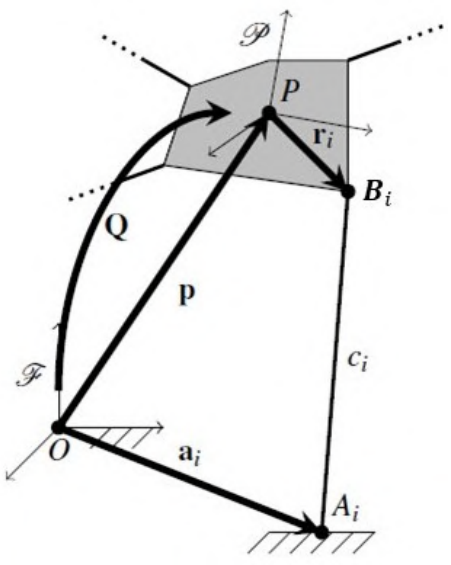

Fig. 5: The kinetostatic model of a CDPR. [24]

- In **Operational Mode 2** ($\mathcal{OM}_2$), the two platforms ($\mathcal{P}_1$ and $\mathcal{P}_2$) are still in contact with each other, but at this stage $\mathcal{P}_1$ is in contact with the ceiling of the workspace, in particular the platform is in contact with one of the docking stations present in the workspace. During $\mathcal{OM}_2$, the two platforms are in static equilibrium and both are stationary $\dot{\mathbf{x}}_1 = \dot{\mathbf{x}}_2 = \dot{\mathbf{x}} = \mathbf{0}$. The mobile platform is defined as $\mathcal{MP} = \mathcal{P}_1 \cup \mathcal{P}_2$,
- In **Operational Mode 3** ($\mathcal{OM}_3$), $\mathcal{P}_1$ is docked to the ceiling of the workspace and is unable to move $\dot{\mathbf{x}}_1 = \mathbf{0}$ (due to the docking system), while $\mathcal{P}_2$ is deployed (disconnected from $\mathcal{P}_1$) $\dot{\mathbf{x}}_2 = \dot{\mathbf{x}}$ and is able to move in a sub-workspace below $\mathcal{P}_1$ with a cylindrical shape. Note that in this phase $\mathcal{P}_2$ can be seen as an underconstrained CDPR with only four cables moving in a 6 DOF environment. Due to this condition, some parasitic motions are expected. During $\mathcal{OM}_3$, the four lower eyelet points of $\mathcal{P}_1$ act as fixed exit points of the "new" sub-CDPR. $\mathcal{MP} = \mathcal{P}_2$.

$\mathcal{P}_2$ during $\mathcal{OM}_3$ is able to reach for example the space between two shelves avoiding cables collision. The three operational mode are shown in Fig. 3.

D. Docking Mechanism

As previously mentioned, the key feature of the $\mathcal{MP}$ is its ability to be attached to the work-cell ceiling using a docking system, allowing $\mathcal{P}_1$ to remain in a fixed position and permitting the deployment of $\mathcal{P}_2$. Two different docking systems were designed, prototyped, and tested on the real robot during this work: the four pins/sockets docking system and the electromagnets driven docking system.

The first method, as shown in Fig. 4a, 4b, consists of four pins attached to the top of $\mathcal{P}_1$ and four sockets attached to the ceiling. The pins and sockets are cone-shaped to ensure a strong connection when fully inserted, but during the approach to the docking, thanks to the conical tip, a small tolerance in the position is tolerated (about 1cm error on the xy plane). The pins/sockets are arranged in a square configuration. The idea of this design is to use the four upper cables to exert a force along the z-axis to hold $\mathcal{P}_1$ and, thanks to the mechanical constraint, to avoid the rotation of $\mathcal{P}_1$ induced by the configuration of the 4 cables.

The second method, as shown in Fig. 4c, 4d, is based on the use of electromagnets to ensure contact and static equilibrium of $\mathcal{P}_1$. In this design, four electromagnets capable to provide 150 Newton of force each, are attached to the top of $\mathcal{P}_1$ and a metal plate (ferromagnetic material) is attached to the ceiling. The electromagnets must be powered, which means that an extra power cable must be connected to the platform. In this approach the upper cables of $\mathcal{P}_1$ are not required to ensure the static equilibrium, in fact in this design all the weight of the $\mathcal{MP}$ is held by the electromagnets. The electromagnets must be activated and released (turned on and off) to dock and undock the platform.

To directly measure the interaction wrench between $\mathcal{P}_1$ and the ceiling, a 6 axis force torque sensor is installed. The sensor is capable of measuring both the interaction force and moment. Using the sensor measurements, it is possible to obtain more consistent data during the experiments. The sensor is an ATI Industrial Automation Delta Sensor [20].

IV. CONTROL STRATEGY

CDPRs, like other types of serial or parallel robots, can be controlled in joint space (JS) or Cartesian space (CS), as well as using a reference value in the pose/twist space or in the wrench space. In particular the main structure of the controller used in this work is based on a set of waypoints defined in CS and connected by fifth order polynomial trajectory, for each time instant a reference values for the $\mathcal{MP}$ pose $\mathbf{x}_d$ twist $\dot{\mathbf{x}}_d$ and acceleration $\ddot{\mathbf{x}}_d$. The control input utilized in this work follows the control strategy presented in [21] and [22]. It consists of three components: a PID based on joints position error, (note that in CDPR this is referred to as the angle of the winches that control the length of the cables) to obtain the desired winch position $\mathbf{q}_d$ and velocity $\dot{\mathbf{q}}_d$ the Inverse Geometric Model (IGM) and Inverse Kinematic Model (IKM) are used while the measured position $\mathbf{q}_m$ is obtained by the motor encoders. The output of the PID is then multiplied by the winch radius R_w to obtain the contribute in term of motor torque Γ_{PID}. A friction compensation term based on the friction model of the motor-gearbox-winch-pulley chain. The last control components, is a Feed-Forward term that depends on the dynamic model of the $\mathcal{MP}$. It is first obtained in the CS and then using a tension distribution algorithm (TDA) is projected in the JS, in particular the barycentric TDA is used [23]. The three obtained components are summed up Γ_{cor} and used as control input. The controller's block diagram is shown in Fig. 6.

However, some modifications have been implemented to handle the reconfigurable $\mathcal{MP}$ and the two presented docking systems. No changes were made to the controller during

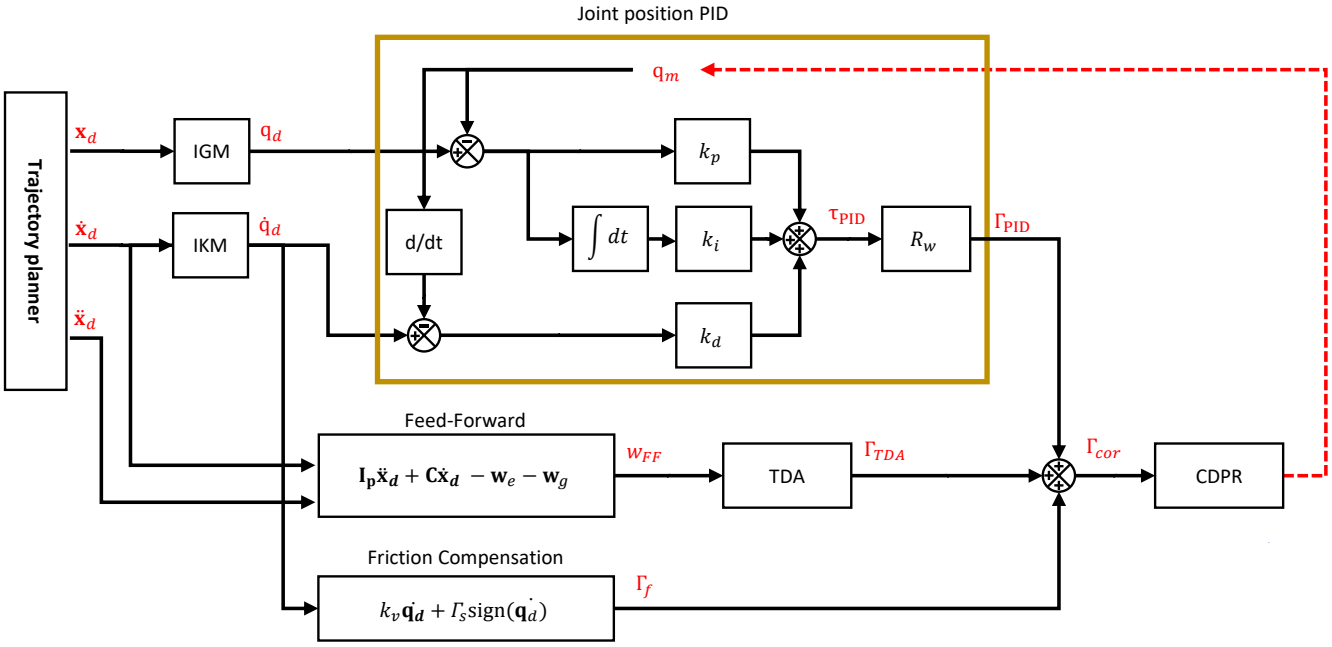

Fig. 6: Block diagram of the main structure of the robot controller.

$\mathcal{OM}_1$. The IGM, IKM, and dynamic model are defined with respect to the $\mathcal{MP}$ ($\mathcal{P}_1 \cup \mathcal{P}_2$). During $\mathcal{OM}_2$ and $\mathcal{OM}_3$, the following modifications are implemented for each docking system to handle the docking phase and deployment of the secondary platform ($\mathcal{P}_2$). Firstly, for both docking system methods, the control of the four upper cables (directly connected to $\mathcal{P}_1$) and the four lower cables are decoupled. Specifically, the lower cables control the $\mathcal{P}_2$ by following a desired CS trajectory based on a set of waypoints. The controller is a simplified version of the one shown in Fig. 6, where the IGM and IKM are related to the $\mathcal{P}_2$ model, and the feed-forward component is reduced to the only gravity compensation term $\mathbf{w}_g$. A different strategy is used to control the four upper cables based on the docking system used. In the four pins/sockets method, the controller must ensure that $\mathcal{P}_1$ exerts a sufficient upward force to maintain the static equilibrium of the platform. This is accomplished by using a reference wrench in CS that is projected in JS using the sub-Wrench matrix i.e., the matrix only considering the contribution of the four upper cables. The sensor installed on top of $\mathcal{P}_1$ is not used as a feedback term for the controller, but solely to acquire data during the experiment. The control strategy for the upper cables in the electromagnets docking system is simpler than the previous one: the controller only keeps the length of the upper cables constant during $\mathcal{OM}_{2/3}$. The controller turn on and off the electromagnets at the appropriate times to ensure a smooth transition. Note that during $\mathcal{OM}_3$, $\mathcal{P}_2$ is not fully constrained as the number of cables is lower than the number of degrees of freedom. However, this condition does not compromise the design's efficiency because, during this phase, $\mathcal{P}_2$ is only required to perform a vertical translation.

V. EXPERIMENTAL VALIDATION

A. Experimental setup

To experimentally verify the effectiveness of the proposed design of a reconfigurable Mobile Platform of a CDPR for pick and place applications, a specific Cartesian trajectory is designed to simulate a P&P scenario, consisting of a series of operations [1]:

1) The $\mathcal{MP}$ is in its home pose Fig. 7a
2) During $\mathcal{OM}_1$, the entire $\mathcal{MP}$ moves under the docking station Fig. 7b
3) The $\mathcal{MP}$ makes contact with the docking station and with respect to the specific docking system used, the $\mathcal{MP}$ will perform the docking ($\mathcal{OM}_2$) Fig. 7c
4) While $\mathcal{P}_1$ is secured to the ceiling, $\mathcal{P}_2$ is deployed and reaches a point under $\mathcal{P}_1$ where it virtually performs its task (pick or place) Fig. 7d
5) Then the process is repeated backward, $\mathcal{P}_2$ is returned to $\mathcal{P}_1$ and the two platforms come into contact with each other
6) The docking system is released
7) The whole $\mathcal{MP}$ moves back to its home pose

These steps, are defined as a set of waypoints with predefined time stamps, connected by a set of polynomial trajectories. The switching between the different controller phases and the activation of the docking system is defined offline. The same

[1] Video of the experiment at **https://youtu.be/QfmYUW-azQM**

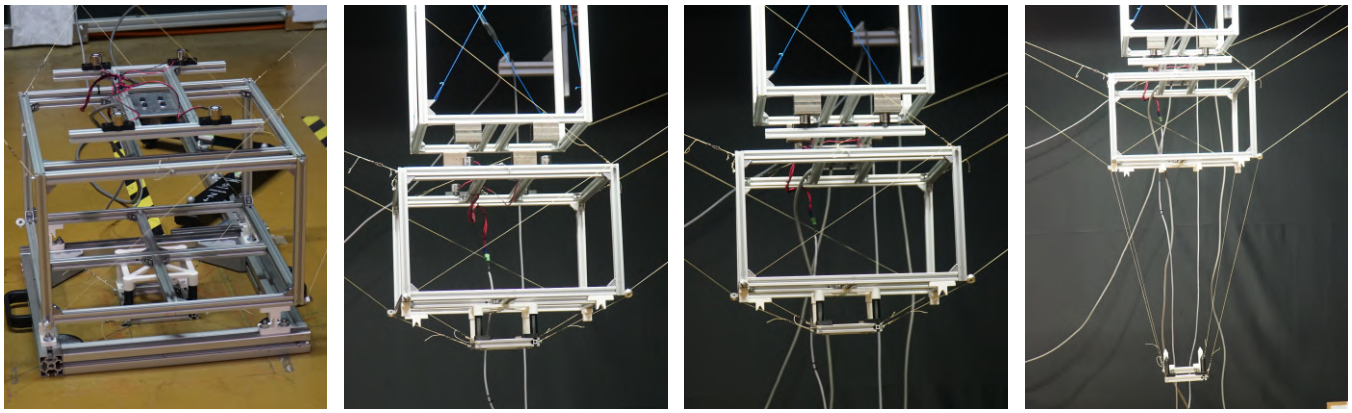

(a) $\mathcal{MP}$ in home pose.

(b) $\mathcal{MP}$ under the docking station ready to dock.

(c) $\mathcal{P}_1$ docked to the ceiling and $\mathcal{P}_2$ ready to be deployed.

(d) $\mathcal{P}_1$ docked, $\mathcal{P}_2$ free to move in its sub-workspace.

Fig. 7: Photos of the main stages of the trajectory defined, to perform the experiment.

trajectory is tested using the two different docking systems to compare their performances. In Fig. 7 the key phases of the experiments are shown.

B. Experimental Results

Fig. 8 illustrates the winch position measurements, providing a clear understanding of how the cables change in length as the platform moves, and shows how the upper (even) and lower (odd) cables are decoupled during the deployment of $\mathcal{P}_2$. Fig. 10 shows the reference tension of each cable demonstrating the varying behavior of the upper and lower cables during the deployment of $\mathcal{P}_2$. Specifically, in Fig. 10a, which refers to the four-pin/socket docking system, the constant tension applied by the upper cables to maintain the static equilibrium of $\mathcal{P}_1$ is visible. Fig. 10b refers to the electromagnet docking system, the tension in the upper cables is kept constant while the docking is ensured by the magnetic force. The plot in Fig. 9 and 11 shows the interaction force and moment between $\mathcal{P}_1$ and the ceiling, as measured by the wrench sensor.

C. Discussion

Both docking methods enable the system to successfully complete the P&P task, even in the presence of close obstacles that would have made it impossible for a traditional CDPR. A comparative table II is presented to highlight the main advantages and disadvantages of each docking system method. Regarding the deployment of $\mathcal{P}_2$, it can be achieved without difficulty using the chosen docking system.

Some clarification can be made about the consideration shown in the table II. The pins/sockets method must be considered as discrete in space because the $\mathcal{MP}$ can only dock in a corresponding of a set of sockets permanently fixed to the ceiling of the workspace. In contrast, the electromagnets can dock anywhere within a metal plate ceiling, allowing more flexibility in choosing the appropriate docking point. A solution that has not been investigated is to compensate the discrete docking of the pins/sockets method moving on x-y plane the $\mathcal{P}_2$ during $\mathcal{OM}_3$, in order to reach the desired target position even if the docking station is imperfectly aligned above the target, this can compensate for misalignment but possible other problems may arise such as parasitic motion in $\mathcal{P}_2$. Note that for simplicity, the prototype ceiling for the electromagnets docking does not provide a wide range docking point, but only a few centimeters of tolerance on the x-y plane.

TABLE II: Main pros and cons of the pins/sockets and the electromagnets docking system studied during this work.

	PROS	**CONS**
pins/sockets	-Simpler design -Completely passive	-More complex control algorithm -Discrete docking system -Smaller workspace for the docking station
electromagnets	-Simpler control algorithm -Continuous docking system position -Bigger workspace for the docking station -Safer connection	-More expensive -Electric power dependent docking

Regarding the workspace dimension where the two methods can perform the docking, some differences are relevant. Since the pins/sockets method must exert a force against the ceiling to ensure docking, the WFW where this force is satisfied is smaller than the WFW where it is not. This results in a smaller working area with respect to the electromagnets system, where the platform only needs to make contact with the ceiling and does not need to exert an additional force to ensure the docking.

Moreover, considering the safety of the docking mechanism during the electromagnet docking, the entire effort is carried out by the electromagnets and therefore, apart from a problem in the powering of the coils, the force is always guaranteed. In contrast, the pins/sockets method relies on the mechanical constraint of the sockets, ensured by the constant tension in the cables; a small lack of tension in the cables or a small elongation in the cables can provoke an undesired undocking of the $\mathcal{P}_1$ and the corresponding fall on the other platform, which can result in serious damage to the structure.

Finally, during $\mathcal{OM}_{2/3}$ of the pins/sockets test, unwanted

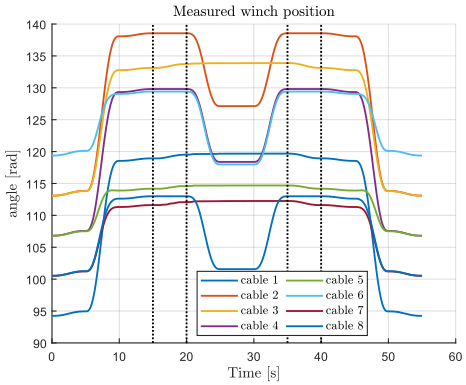

(a) Pins/sockets docking system

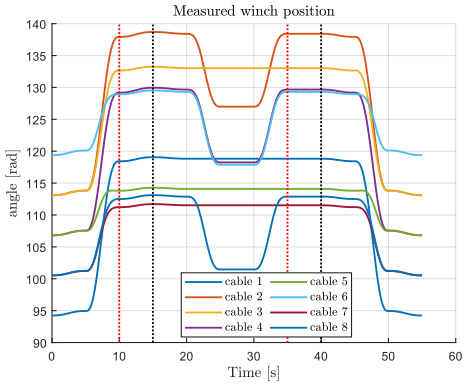

(b) Electromagnet driven docking system

Fig. 8: Behavior of the winches position angles during the experiment. Note that the black dotted lines represent the translation between the different $\mathcal{OM}$, while the red dotted lines represent the instant in which the electromagnets are turned on/off.

forces along the x-y plane can be observed, mainly due to the four pins/sockets structure mounted between the sensor and the pins. This structure does not guarantee a symmetrical and uniform distribution of the contact forces.

VI. CONCLUSION

In this work, the design and prototype of a reconfigurable mobile platform for Cable-Driven Parallel Robots was presented. The tests yielded results regarding the feasibility of the idea and demonstrated an improvement in the reachability of the $\mathcal{MP}$ in a cluttered environment. Further research is necessary to conduct a deeper analysis of the robot workspace. To accurately determine the WFW of the robot, it is important to analyze its behavior both as a single platform and when $\mathcal{P}_1$ is docked and $\mathcal{P}_2$ is free to move. This analysis should consider the robustness of different docking systems and their contribution to the shaping of the WFW. Studies must be carried out on a trajectory planner capable of managing an optimal strategy during the pick-and-place task to optimize when the displacement of $\mathcal{P}_2$ is necessary and which can be the best docking position in order to perform a desired task without colliding with the environment. Finally, a more advanced controller will be synthesized to consider the feedback provided by the force and torque sensor during the docking phase.

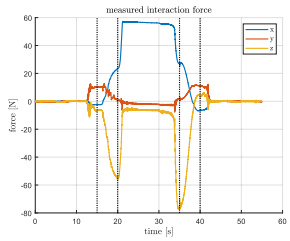

(a) Interaction force, the z-axis has two spikes during the $\mathcal{MP}$ gets in contact with the ceiling and when it lost the contact. There is a consistent force along the x-axis during $\mathcal{OM}_3$ probably due to the shape of the pins support.

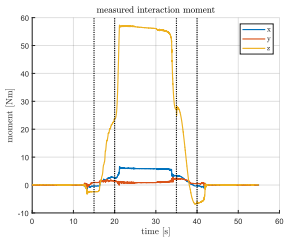

(b) Interaction moment, a consistent moment about z-axis is generated by the four upper cables during $\mathcal{OM}_{2/3}$, some noise is present about x and y axes during $\mathcal{OM}_{2/3}$.

Fig. 9: Interaction wrench in the pins/sockets docking system experiment.

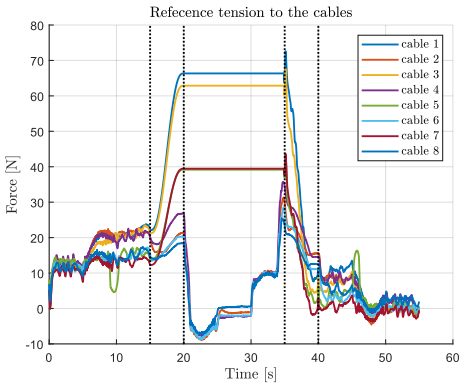

(a) Pins/sockets docking system.

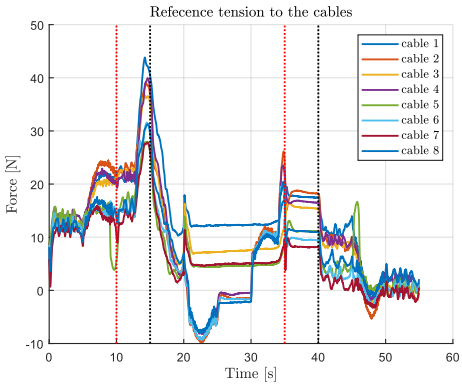

(b) Electromagnet driven docking system

Fig. 10: Behavior cables tension during the experiment.

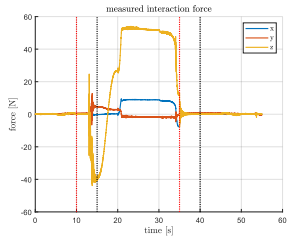

(a) Interaction force measured. The first spike is due to the contact, the plateau correspond to the weight of the $\mathcal{P}_1$ itself.

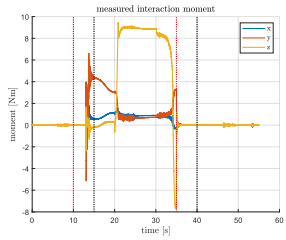

(b) Interaction moment measured.

Fig. 11: Interaction wrench in the electromagnets driven docking system experiment.

REFERENCES

[1] Pott, Andreas. Cable-driven parallel robots. Ed. Tobias Bruckmann. Berlin/Heidelberg, Germany: Springer, 2013.

[2] Stewart D. A Platform with Six Degrees of Freedom. Proceedings of the Institution of Mechanical Engineers. 1965;180(1):371-386.

[3] Skopin Matthew, Philip Long, and Taskin Padir. "Design of a docking system for cable-driven parallel robot to allow workspace reconfiguration in cluttered environments." International Conference on Cable-Driven Parallel Robots. Cham: Springer International Publishing, 2021.

[4] Skycam, https://en.wikipedia.org/wiki/Skycam, visited on January 24 2024.

[5] A. Pott, C. Meyer and A. Verl, "Large-scale assembly of solar power plants with parallel cable robots", Isr/Robotik 2010, pp. 999-1004, 2010.

[6] R. Yao, X. Tang, J. Wang and P. Huang, "Dimensional optimization design of the four-cable-driven parallel manipulator in fast", IEEE/ASME Transactions on Mechatronics, vol. 15, no. 6, pp. 932-941, 2010.

[7] Jean-Baptiste Izard, Marc Gouttefarde, Cédric Baradat, David Culla, Damien Sallé. Integration of a parallel cable-driven robot on an existing building façade. 1st International Conference on Cable-Driven Parallel Robots (2012), 2012, Stuttgart, Germany. pp.149-164.

[8] A. Zargari, Z. A. Castrejon, D. Kim and P. Y. Oh, "Cable-Driven Parallel Robot for Warehouse Monitoring Tasks," 2023 IEEE 13th Annual Computing and Communication Workshop and Conference (CCWC), Las Vegas, NV, USA, 2023, pp. 1085-1090.

[9] É. Picard, S. Caro, F. Claveau and F. Plestan, "Pulleys and Force Sensors Influence on Payload Estimation of Cable-Driven Parallel Robots," 2018 IEEE/RSJ International Conference on Intelligent Robots and Systems (IROS), Madrid, Spain, 2018, pp. 1429-1436.

[10] Rousseau, Thomas, Christine Chevallereau, and Stéphane Caro. "Human-cable collision detection with a cable-driven parallel robot." Mechatronics 86 (2022): 102850.

[11] Izard, JB., Dubor, A., Hervé, PE. et al. Large-scale 3D printing with cable-driven parallel robots. Constr Robot 1, 69–76 (2017).

[12] Khajepour, Amir, et al. "A Warehousing Robot: From Concept to Reality." International Conference on Cable-Driven Parallel Robots. Cham: Springer Nature Switzerland, 2023.

[13] Pedemonte, Nicolò, et al. "Fastkit: A mobile cable-driven parallel robot for logistics." Advances in Robotics Research: From Lab to Market: ECHORD++: Robotic Science Supporting Innovation (2020): 141-163.

[14] Lamine, Houssein, Sami Bennour, and Lotfi Romdhane. "Design of cable-driven parallel manipulators for a specific workspace using interval analysis." Advanced Robotics 30.9 (2016): 585-594.

[15] Bouchard, Samuel, Clément Gosselin, and Brian Moore. "On the ability of a cable-driven robot to generate a prescribed set of wrenches." (2010): 011010.

[16] Bosscher, Paul, Andrew T. Riechel, and Imme Ebert-Uphoff. "Wrench-feasible workspace generation for cable-driven robots." IEEE Transactions on Robotics 22.5 (2006): 890-902.

[17] Rasheed, Tahir, Philip Long, and Stéphane Caro. "Wrench-feasible workspace of mobile cable-driven parallel robots." Journal of Mechanisms and Robotics 12.3 (2020): 031009.

[18] Rasheed, Tahir, et al. "Wrench Capability Analysis of a Planar Dual-Platform Cable-Driven Parallel Robot." International Design Engineering Technical Conferences and Computers and Information in Engineering Conference. Vol. 87363. American Society of Mechanical Engineers, 2023.

[19] J. Lamaury, M. Gouttefarde, A. Chemori and P. -É. Hervé, "Dual-space adaptive control of redundantly actuated cable-driven parallel robots," 2013 IEEE/RSJ International Conference on Intelligent Robots and Systems, Tokyo, Japan, 2013, pp. 4879-4886

[20] ATI Industrial Autonation, https://www.ati-ia.com/index.aspx, visited on January 25 2024.

[21] Johann Lamaury. Contribution à la commande des robots parallèles à câbles à redondance d'actionnement. Automatique / Robotique. Université Montpellier II - Sciences et Techniques du Languedoc, 2013. Français.

[22] Picard, E., Plestan, F., Tahoumi, E., Claveau, F. and Caro, S., 2021, "Control Strategies for a Cable-Driven Parallel Robot with Varying Payload Information", Mechatronics, Elsevier, 2021, Vol. 79, pp. 102648.

[23] Mikelsons, Lars, et al. "A real-time capable force calculation algorithm for redundant tendon-based parallel manipulators." 2008 IEEE International Conference on Robotics and Automation. IEEE, 2008.

[24] Ana Lucia Cruz Ruiz, Stéphane Caro, Philippe Cardou, François Guay. ARACHNIS: Analysis of Robots Actuated by Cables with Handy and Neat Interface Software. Cable-Driven Parallel Robots, Mechanisms and Machine Science, 32, Springer, pp.293-305, 2015.